nature physics

Article

https://doi.org/10.1038/s41567-022-01858-8

Long-lived Andreev states as evidence for protected hinge modes in a bismuth nanoring Josephson junction

Received: 13 December 2021

Accepted: 28 October 2022

Published online: 16 January 2023



A. Bernard¹, Y. Peng^{2,3}, A. Kasumov^{1,4}, R. Deblock ¹, M. Ferrier¹, F. Fortuna⁵, V. T. Volkov⁴, Yu. A. Kasumov⁴, Y. Oreg ⁶, F. von Oppen⁷, H. Bouchiat¹ & S. Guéron ¹

Second-order topological insulators are characterized by helical, non-spin-degenerate one-dimensional states running along opposite crystal hinges with no backscattering. Injecting superconducting pairs therefore entails splitting Cooper pairs into two families of helical Andreev states of opposite helicity, one at each hinge. Here we provide evidence for such separation via the measurement and analysis of the switching supercurrent statistics of a crystalline nanoring of bismuth. Using a phenome nological model of two helical Andreev hinge modes, we find that pairs relax at a rate comparable to individual quasiparticles, in contrast to the much faster pair relaxation of non-topological systems. This constitutes a unique telltale sign of the spatial separation of topological helical hinges.

Soon after the discovery of one-dimensional (1D) helical states in two-dimensional topological insulators (2D TIs)^{1,2} or three-dimensional (3D) second-order TIs (SOTIs)^{3–5}, it was realized that Josephson junctions containing helical modes as their weak link should display remarkable features. Indeed, the spin-momentum locking that characterizes the helical states translates into a fixed helicity for the Andreev states shuttling the supercurrent along each edge, in contrast to the spin degeneracy of conventional Josephson junctions. Among the predicted consequences are 4π (refs. 6,7) and 8π (refs. 8,9) periodicities of the supercurrent-phase relation (CPR) of a Josephson junction with a single helical edge state. Originating from fermion-parity-protected crossings of Andreev levels at phase difference π , these periodicities are contingent on the absence of fermion-parity-breaking processes. The necessity to overcome such relaxation processes motivated the initial search for topological signatures at finite frequencies.

Previous measurements relied on the a.c. Josephson effect via Shapiro steps¹⁰ and Josephson emission of voltage-biased junctions¹¹ or,

as suggested in ref. ⁷, on the high-frequency response of a phase-biased topological junction¹². Recent theoretical predictions suggest that signatures of topological superconductivity can also be found in switching current experiments conducted at frequencies comparable to the relaxation rate^{13–16}. The idea is that the current at which the junction switches to its resistive state depends on the number and occupation of the current-carrying Andreev states. This implies that detailed information about the Andreev states and relaxation processes can be extracted from the phase-dependent statistical distributions of switching currents^{14,17}. The particular sawtooth-like shape of the CPR makes long Josephson junctions with multiple sub-gap Andreev levels especially well suited to such investigations^{15,18}.

In this Article we report measurements of the switching current distribution of a micrometre-sized ring-shaped Bi monocrystal with superconducting contacts (Fig. 1a). It was recently suggested ¹⁹ and corroborated by experiments ^{12,20–26} that Bi is a SOTI with helical modes propagating along its hinges. We found that in our device the Bi ring acts

¹Laboratoire de Physique des Solides, Université Paris-Saclay, CNRS, Orsay, France. ²Department of Physics and Astronomy, California State University, Northridge, Northridge, California, USA. ³Institute of Quantum Information and Matter and Department of Physics, California Institute of Technology, Pasadena, California, USA. ⁴Institute of Microelectronics Technology and High Purity Materials RAS, Chernogolovka, Moscow Region, Russia. ⁵Institut des Sciences Moléculaires d'Orsay, Université Paris-Saclay, CNRS, Orsay, France. ⁶Department of Condensed Matter Physics, Weizmann Institute of Science, Rehovot, Israel. ⁷Dahlem Center for Complex Quantum Systems and Fachbereich Physik, Freie Universität Berlin, Berlin, Germany.
©e-mail: sophie.gueron@universite-paris-saclay.fr

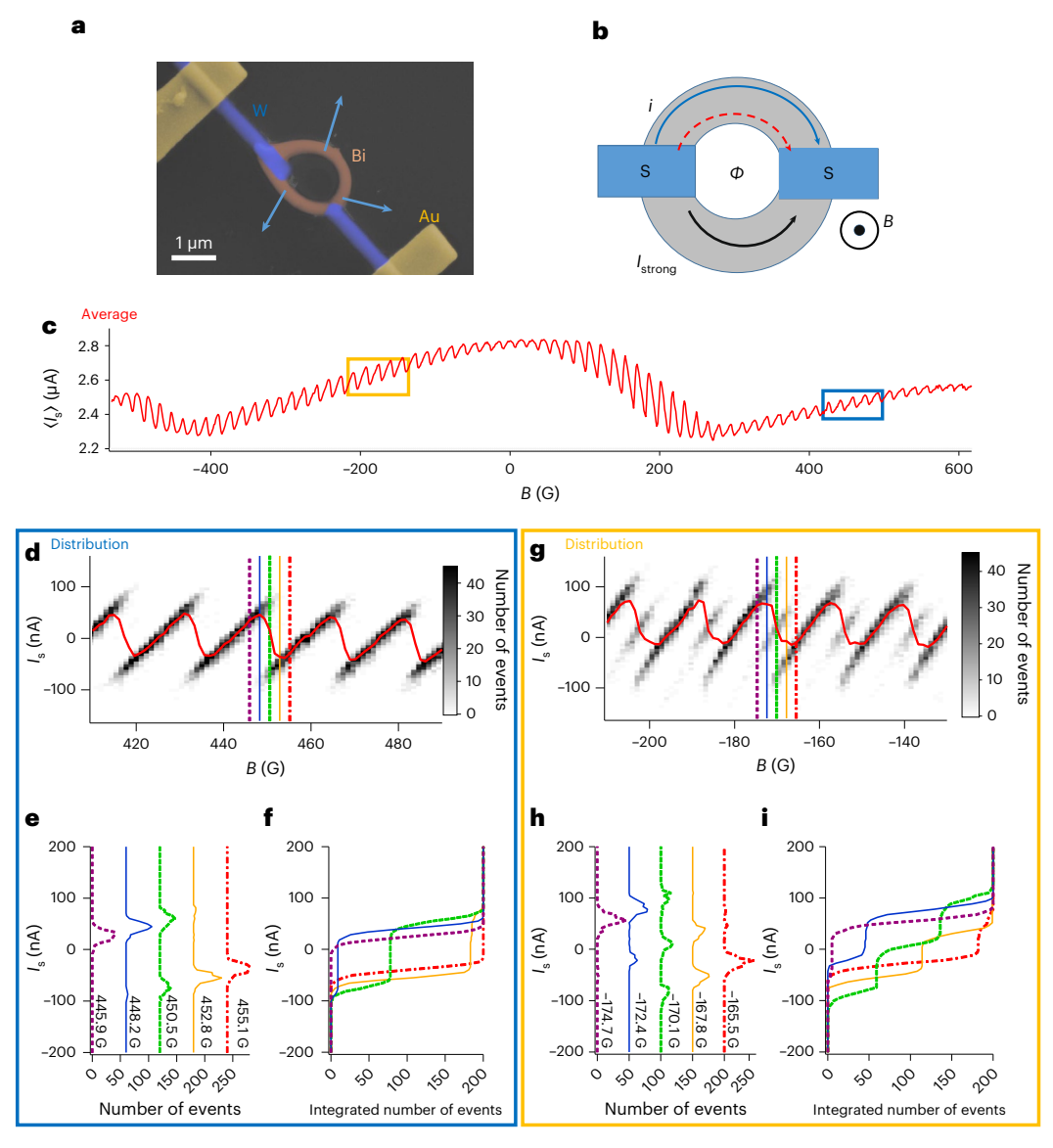


Fig. 1 | Comparison of average and distribution of switching currents of the asymmetric bismuth SQUID. a, False-colour scanning electron micrograph of the Biring (brown) with superconducting W contacts (blue) and Au leads (yellow). The crystalline [111] axis (blue arrows) was found to maintain a radial orientation (Methods). b, Sketch of the Bi nanoring connected to two superconducting contacts (S), forming an intrinsic SQUID. In the model, the total supercurrent splits into a small supercurrent i carried by two helical channels (solid blue and dashed red arrows) in one branch of the ring, and a high supercurrent I_{strong} in the other branch. The magnetic field B induces a flux ϕ through the loop. \mathbf{c} , Average switching current (I_s) measured with a bias current ramp of 17 Hz as a function of $B.\langle I_s \rangle$ displays a slightly rounded, sawtooth-shaped modulation with both signs of skewness, as well as regions where the modulation is more symmetric than a sawtooth (for example, at approximately zero field). Note the asymmetry with field, which is related to the Josephson diode effect (Supplementary Fig. 2). d,g, Comparison of the average (red lines) and full distribution (with the number of switching events coded in shades of grey) of the switching current in 450 G (d)

and -170 G (g) fields for a current ramp of 17 Hz (coloured boxes in c). The baseline due to I_{strong} has been subtracted. The average switching current curves are rounded. In contrast, in d, the distribution contains no switching events in the sawtooth discontinuities. Interestingly, there are regions around the discontinuities where two different switching currents are possible, as best seen in the histograms (e) and integrated histograms (f) extracted at the fields indicated by the coloured vertical lines in (d). Curves in (e) have been shifted horizontally for clarity. g, At -170 G, the switching current distributions display intermediate fainter branches, leading to some field regions where three values of the switching current are possible. This is visible in the histograms (h) and integrated histograms (i) taken at the field values indicated by the coloured vertical lines in (g). Curves in (h) have been shifted horizontally for clarity. In the text, we argue that all features are well explained by the field-dependent occupation of Andreev states of two supercurrent-carrying helical hinges in the weak Josephson branch of the ring. The statistical error on all quantities is $1/\sqrt{N} \simeq 7\%$, where N = 200 is the number of measurements at each flux.

as an intrinsically asymmetric superconducting quantum interference device (SQUID) whose average switching current yields the characteristic sawtooth CPR of a long ballistic junction. In addition, by careful comparison to a phenomenological model, we show that the observed switching current behaviour corroborates the existence of helical hinge modes in Bi. Our analysis leads to the identification of single-particle

and two-particle relaxation times, both of the order of milliseconds, which are consistent with well-separated topological hinge modes.

The average switching current at low fields, shown in Fig. 1c, displays periodic oscillations superimposed on a slowly varying baseline (see Methods and Supplementary Figs. 1–4). The 17 G period, corresponding to a superconducting flux quantum $\Phi_0 = h/2e$ over an area of 1.2 μ m², is

consistent with the ring area. The oscillations have a (slightly rounded) sawtooth shape, which is reminiscent of switching experiments on asymmetric SQUIDs designed to measure the CPR of small Bi nanowire junctions²³. The sawtooth modulation corresponds to the CPR of a long ballistic Josephson junction, and thus demonstrated the higher-order topological nature of the Bi nanowire^{18,19,23,27}. In this experiment, the sawtooth modulation suggests that the Bi ring, with its two superconducting contacts, acts intrinsically as an asymmetric SQUID, yielding a ballistic CPR for the branch of the ring with the smaller critical current.

Instead of the average switching current, this Article focuses on the switching current distribution, which is arguably a much more powerful (and underexploited) tool. We show that the distribution reveals the phase dependence of the ground and excited states of the Andreev spectrum, their occupation probability and spatial separation, and hence their topological character. Two such distributions, recorded in two magnetic field regions, are displayed in Fig. 1d,g. In contrast to the average, the switching current distributions are not rounded as a function of field. In the first magnetic field region, around B = 450 G, a notable feature of the sawtooth jump region is the two well-separated peaks in the histogram (green curve in Fig. 1e). This indicates that the weak junction can be in two different states on the timescale of the current ramp. In the second field region, near $B = -170 \,\mathrm{G}$ (Fig. 1g), an additional intermediate, fainter branch develops around the sawtooth jump, resulting in three well-separated peaks in the switching histograms (green curve in Fig. 1h). Correspondingly, the integrated switching current distributions display one (Fig. 1f) or two (Fig. 1i) intermediate plateaux. In the following, we argue that each peak in the histogram corresponds to a different occupation of the Andreev spectrum of a Josephson junction made of two helical hinges. Our analysis then yields the relative relaxation rates of the Andreev states, providing information about the topological character of these hinges.

The analysis is based on a model of the Bi ring connected to two superconducting contacts as a SOTI-based asymmetric SQUID. In this model, the weak Josephson junction consists of two helical supercurrent-carrying hinges located in one branch of the ring, and the strong junction (with a higher critical current) is formed by the other branch (Fig. 1b). To leading order, the time-dependent current ramp $\mathcal{I}(t)$ controls the phase difference $\gamma(t)$ across the strong junction. As \mathcal{I} increases from zero to values close to the strong junction's critical current $I_{c,\text{strong}}$, γ increases from zero to γ_{max} . Owing to the flux threading the SQUID Φ (in units of $\hbar/(2e)$), the phase difference across the weak junction is $\phi(t) = \Phi + \gamma(t)$. The additional current through the weak junction with CPR $i(\phi)$ modulates the critical current when the SQUID switches to a resistive state: $I_{c} \simeq I_{c,\text{strong}} + i(\Phi + \gamma_{\text{max}})$. The SQUID's switching current thus provides a direct measurement of the CPR of the weak junction $i^{4,17,28}$.

The CPR $i(\phi)$ reflects the Andreev spectrum and, importantly, its occupation as a function of the phase difference ϕ (ref. 18). Let us first consider the case of a junction made of a single hinge, as sketched in Fig. 2a-c. Figure 2a,b displays the single-particle and many-body Andreev spectra. The many-body spectrum exhibits level crossings at integer multiples of π . The crossings at odd multiples are protected by fermion-parity conservation, whereas those at even multiples require time-reversal symmetry. Fermion-parity-violating processes are suppressed if a hinge mode is sufficiently isolated from other hinge modes or single-electron impurity states. To simplify, we focused on the two lowest-energy many-body states, whose CPRs, $i_g(\phi)$ for the ground state and $i_e(\phi)$ for the excited state, are sketched in Fig. 2c. Both are piecewise linear and 2π -periodic functions 16,18,29 . We next considered the case of two hinges. Given that each hinge can be either in the ground or excited state, there are four possible states for the system, gg, ee, eg and ge, whose CPR is $i_{l'} = i_l(\phi) + i_{l'}(\phi)$, where l and l' are g or e (Fig. 2d). In the case of two hinge channels in the long junction regime, with same critical currents, $i_{gg} = 2i_g$, $i_{ee} = 2i_e$ and $i_{ge}(\phi) = i_{eg}(\phi) = i_{gg}(\phi) + i_{eg}(\phi) = i_{gg}(\phi)$ $+\pi$), which is the sawtooth-shaped CPR of the ground state shifted by π . The three different CPRs are sketched in Fig. 2d.

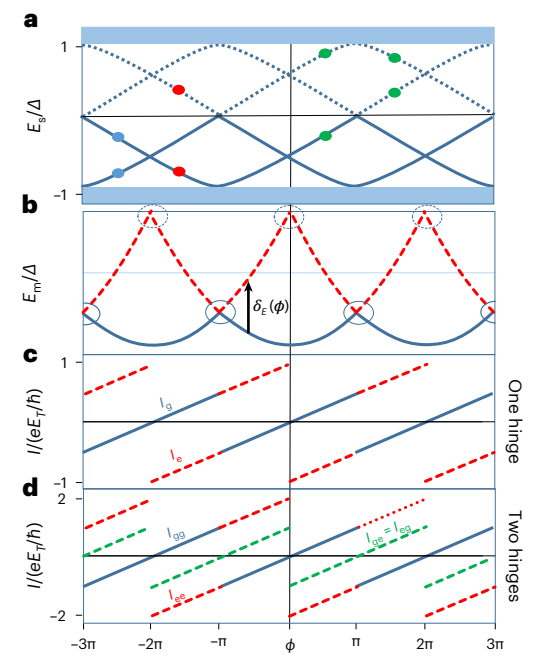


Fig. 2 | Andreev spectrum and Josephson current of an intermediate-length Josephson junction with one or two helical hinges between superconducting electrodes. a, Andreev spectrum of single-particle (Bogoliubov-de Gennes) excitations E_s for a single-hinge mode, where Δ is the pair potential. In the ground state, the two negative-energy states are occupied (blue circles). The lowest positive-energy state is occupied in the first excited state (and thus the corresponding negative-energy state is empty; red circles). Higher-energy excited states are indicated by green circles (but not included in our theoretical model). Solid and dashed lines correspond to positive and negative energy, respectively. The blue shaded regions represent the above-gap continuum. **b**, Andreev spectrum of corresponding many-body states E_m (given by the sum of Andreev levels and the continuum), including the ground state $E_g(\phi)$ (solid blue line) and the first excited state $E_{\rm e}(\phi)$ (dashed red line). The excitation energy $\delta_E(\phi) = E_e(\phi) - E_e(\phi)$ is indicated by an arrow. Level crossings at odd multiples of π (solid rings) are protected by fermion parity, while level crossings at even multiples of π (dashed rings) are protected by time-reversal symmetry (strictly speaking, these are broken by the magnetic field in the experiment). **c**, Corresponding Josephson currents $i_g(\phi)$ in the ground state (solid blue line) and $i_e(\phi)$ in the first excited state (dashed red line), given by the derivative of the many-body energies with respect to ϕ . i_g is linear between $-\pi$ and π , with downward jumps by $ev_F/L \equiv \frac{e}{\hbar}E_T$ at $\phi = \pi + 2\pi n$ ($n \in \mathbb{Z}$), where $E_T = \hbar v_F/L$ is the Thouless energy, v_F is the Fermi velocity of the hinge mode and L is the distance between the two superconductors. For the excited state, i_e is also linear, with downward jumps by $2ev_F/L$ at $\phi = 2\pi n$ and upward jumps by ev_F/L at $\phi = \pi + 2\pi n$. d, Josephson currents of a junction with two (identical) hinge modes. The current equals $i_{gg}(\phi) = 2i_{g}(\phi)$ when both hinges are in their ground states (solid blue line), $i_{\rm eg}(\phi) = i_{\rm ge}(\phi) = i_{\rm g}(\phi) + i_{\rm e}(\phi)$ when one hinge is in the excited state (dashed green line) and $i_{ee}(\phi) = 2i_e(\phi)$ (dashed red line) when both are excited.

In the following, we use this model to compute the occupation probability of the various Andreev levels that matches the one extracted from the experimental switching current distribution. To this end, we first solved the rate equations for the probabilities $p_{\rm gg}$, $p_{\rm ge} = p_{\rm eg}$ and $p_{\rm ee}$ of occupying states gg, eg/ge, and ee, respectively. The rate equations are:

$$\frac{dp_{gg}}{dt} = -2\Gamma_{eg \leftarrow gg}p_{gg} + 2\Gamma_{gg \leftarrow eg}p_{eg} - \Gamma_{ee \leftarrow gg}p_{gg} + \Gamma_{gg \leftarrow ee}p_{ee}
\frac{dp_{eg}}{dt} = -\Gamma_{gg \leftarrow eg}p_{eg} + \Gamma_{eg \leftarrow gg}p_{gg} - \Gamma_{ee \leftarrow eg}p_{eg} + \Gamma_{eg \leftarrow ee}p_{ee},$$
(1)

where $p_{ee} = 1 - 2p_{eg} - p_{gg}$. They include two types of relaxation process, sketched in Fig. 3b,c. The intra-hinge poisoning processes cause one

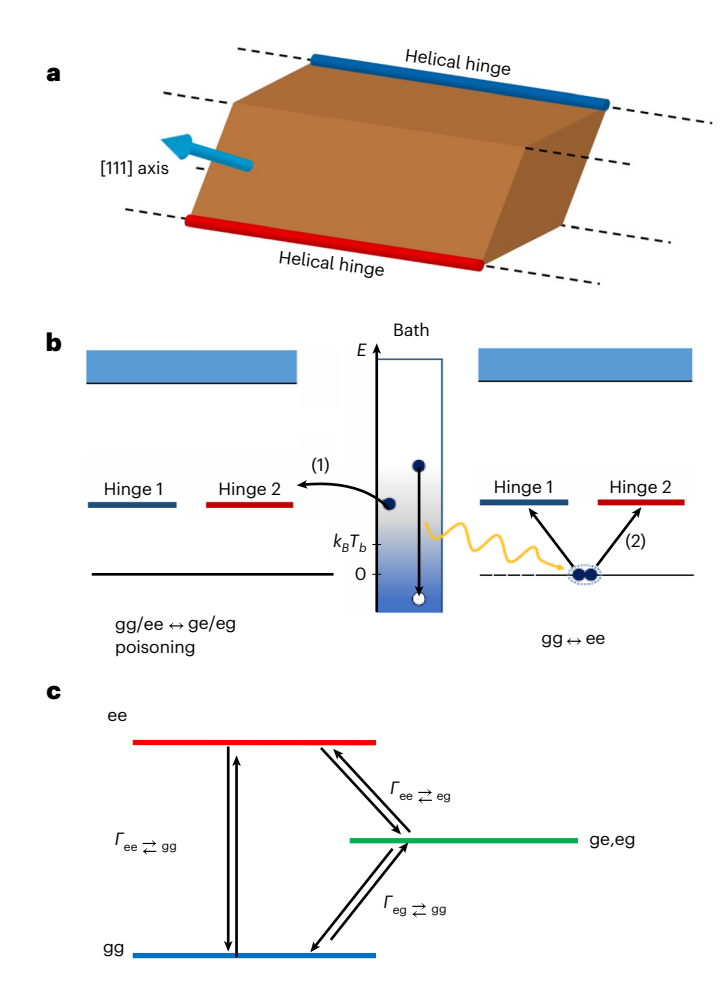


Fig. 3 | Excitation processes in the case of two spatially separated helical Andreev hinge states, a. Sketch of a segment of the ring with a radial [111] axis (light blue arrow) and two helical hinge channels of opposite helicities on separate hinges (red and blue lines). b, Quasiparticle and pair excitation processes. The dashed horizontal lines at zero energy represent the superconducting ground state that acts as a Cooper pair reservoir. The blue region above energy ∆ represents the quasiparticle continuum. The dark blue and red horizontal lines represent in-gap non-spin-degenerate helical Andreev bound states energy levels at a fixed ϕ , each associated to a single helical (hinge) mode. Arrows represent processes that transfer one-particle occupation between two states. The intra-hinge or poisoning process (1) involves only one hinge and the quasiparticle bath, and the exchange of a quasiparticle that changes the parity of the hinge 17,29,30. The inter-hinge or pair process (2) involves two hinges, energy $2\delta_F$ from the bath and a Cooper pair from the superconducting condensate. It does not change the global parity of the two-hinge system. This process is slower in the case of two separate helical hinges than in the case of one spin-degenerate non-helical channel. c, Andreev energy levels of the two-hinge junction and corresponding relaxation rates.

hinge to be excited or relax with either a rate $\Gamma_{\text{ee} \neq \text{ge}}$, involving a relaxation time τ_1 , or $\Gamma_{\text{eg} \neq \text{gg}}$, involving a relaxation time τ_1 . The inter-hinge pair processes with rates $\Gamma_{\text{gg} \neq \text{ee}}$, in which two quasiparticles from different hinges condense into a Cooper pair (or a Cooper pair splits to populate the two hinges), involve a pair relaxation time τ_p . Following ref. ¹³, we assumed that the intra-hinge transition rates involve a fermionic bath at temperature T_{qp} : $\Gamma_{\text{ee} \neq \text{eg}}(\phi) = f(\pm \delta_{\mathcal{E}}(\phi)/k_{\text{B}}T_{\text{qp}})/\tau_2$, where f is the Fermi distribution function, k_{B} is the Boltzmann constant and $\delta_{\mathcal{E}}(\phi) = E_{\text{e}}(\phi) - E_{\text{g}}(\phi)$ is the gap between the ground and excited states. Similarly, $\Gamma_{\text{eg} \neq \text{gg}}(\phi) = f(\pm \delta_{\mathcal{E}}(\phi)/k_{\text{B}}T_{\text{qp}})/\tau_1$. The inter-hinge or pair rates also involve a fermionic bath at a temperature T_{b} (this can be different from T_{qp}). These inter-hinge relaxation processes do not require external particles from the fermionic bath, only energy. The rates thus contain

the Bose–Einstein function and twice the excitation energy $2\delta_{\epsilon}(\phi)$. They are suppressed for hinge modes that are far apart in real space on the scale of the superconducting coherence length.

$$\Gamma_{\text{ee} \Rightarrow \text{gg}} = \frac{2\delta_{E}(\phi)}{E_{T}\tau_{\text{p}}} \begin{cases} n_{B} \left(\frac{2\delta_{E}(\phi)}{k_{\text{B}}T_{\text{b}}}\right) \\ 1 + n_{B} \left(\frac{2\delta_{E}(\phi)}{k_{\text{B}}T_{\text{b}}}\right), \end{cases}$$

where $n_B(x) = (e^x - 1)^{-1}$ is the Bose function. The probabilities were obtained by numerically integrating equation (1) from $\phi = \Phi$ to $\phi_{sw} = \Phi + \gamma_{max}$, assuming that $\gamma(t)$ increases linearly in time, $\gamma(t) = \omega t$ from 0 to γ_{max} as $\mathcal{I}(t)$ ramps up from 0 to I_c . We selected $\gamma_{max} = \pi/2$, which best fitted the experimental data (Supplementary Fig. 5 for $\gamma_{max} = \pi$). The initial conditions were the equilibrium probabilities (see details in the Supplementary Information). From the probabilities of occupying the different states, we computed the probability of switching to a dissipative state. The switching current statistical distribution was then generated, taking into account the fact that for a given state, switching is a stochastic event characterized by a current probability distribution. We thus introduced a state-dependent switching probability $P_{\rm sw}^{l,l'}(I,\phi_{\rm sw})$, which is the probability of finding the SQUID in the resistive state at bias current I and switching superconducting phase difference $\phi_{sw'}$ for a given occupied state ll'. We approximated $P_{sw}^{l,l'}(I,\phi_{sw})$ using a smoothed step function of width δ /centred around the SQUID's critical current $I_c^{ll'} = I_c^l + I_c^{l'}$ (which depends on the state of the weak junction through $i_{l,l'}(\phi_{sw})$). The total switching probability is then expressed as $P(I, \phi) = \sum_{l,l' \in \{e,g\}} p_{ll'}(\phi) P_{sw}^{ll'}(I, \phi)$.

To compare experiment and theory, we extracted the field-dependent histograms and integrated histograms from the experimental switching current distributions, from which we derived the state-dependent experimental occupation probabilities (Methods). The theoretical occupation probabilities were then computed using the parameters $\omega \tau_1$, $\omega \tau_2$, $\omega \tau_p$, T_b and T_{qp} , which best reproduced the experimental occupation probabilities. $P_{sw}^I(I, \phi_{sw})$, $dP(I, \phi_{sw})$ /dI and the full switching distribution as a function of flux were subsequently generated using these parameters.

Figure 4 shows how well the experimental switching current distribution around -170 G was reproduced by theory. Two current ramp frequencies, 17 and 187 Hz, were investigated. The model reproduced the extent to which the fainter intermediate (poisoning) branch extended. and how it extended further in the case of the higher current ramp frequency. The model also reproduced the shape, height, and relative positions of the three probability distributions (p_{gg} , p_{eg} + p_{ge} and p_{ee} , extracted from the integrated experimental histogram) remarkably well; compare Fig. 4b, f and Fig. 4d, h. In the regions with three possible switching currents, there are three non-negligible occupation probabilities of the states gg, ee and eg. For the slowest ramp, p_{gg} and p_{ee} were extremal at π , whereas $p_{eg} + p_{ge}$ was maximal slightly above π (Fig. 4f). The corresponding plot at a ramp frequency 11 times greater, Fig. 4h, shows a much greater shift of the maximum of $p_{eg} + p_{ge}$. This shift is the signature of the inter-hinge pair relaxation processes at τ_p . The parameters used were $\tau_{\rm qp} = \tau_1 = \tau_2 = 10.5$ ms and $\tau_{\rm p} = 1.82$ ms for both the slow and fast ramps. Only $T_{\rm b} = T_{\rm qp}$ was allowed to change, yielding $k_{\rm B}T_{\rm b}/E_{\rm T} \simeq 0.4$ for 17 Hz and $k_{\rm B}T_{\rm b}/E_{\rm T} \simeq 0.7$ for 187 Hz, reflecting the shorter time available for quasiparticle thermalization in the reservoirs. We estimated a factor of two uncertainty for $\tau_{\rm qp}$ and five for $\tau_{\rm p}$, and thus a factor of seven uncertainty for the ratio τ_{qp}/τ_p (see Supplementary Figs. 5 and 6 for the effects of the different parameters and the precision with which they could be estimated).

We next turned to modelling the experimental switching current distribution around 450 G (Fig. 5). Interestingly, in this field region, hardly any intermediate switching branch is visible (Fig. 5a). This meant that the ee and gg states were much more populated than the eg state, as clearly shown in the extracted occupation probabilities (Fig. 5b,d):

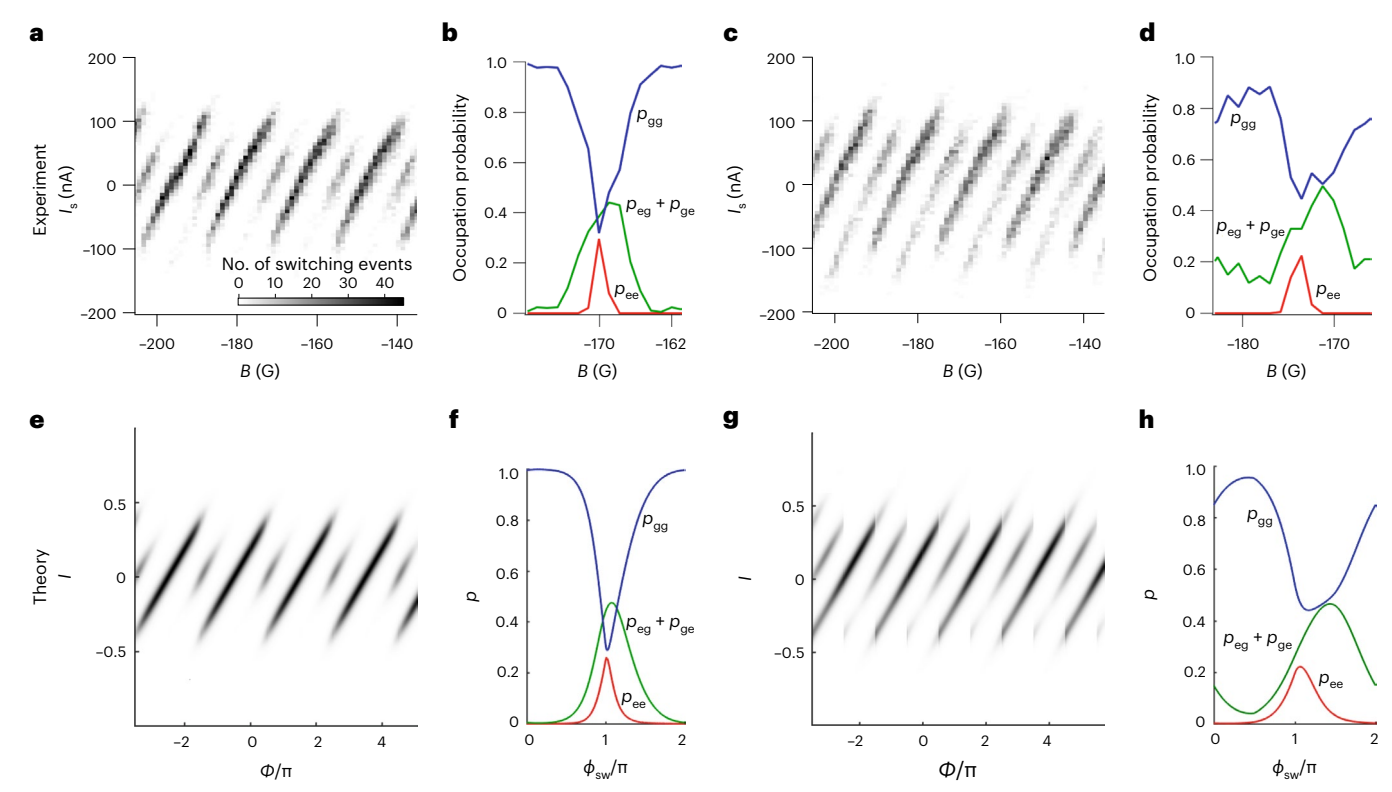


Fig. 4 | Comparison of the experimental switching statistics and extracted Andreev hinge state occupation probabilities to the results of the theoretical model in a field region centred at -170 G. a-d, Experiment. e-h, Theory. a,c, Switching current histograms over four flux periods at ramp frequencies of 17 Hz (a) and 187 Hz (c). A linear dependence has been subtracted to remove the critical current of the strong junction. **b**,**d**, Field dependence of the occupation probability of three configurations, corresponding to both hinges in the ground state $(p_{gg}, blue)$, both hinges in the excited state (p_{ee}, red) or one hinge in the ground state and the other in the excited state ($p_{\rm eg}$ + $p_{\rm ge}$, green) at 17 Hz ($\bf b$) and 187 Hz (d). The statistical error on all quantities is $1/\sqrt{N} \simeq 7\%$, where N = 200 is the number of measurements at each flux. The corresponding theoretical curves are computed (see Methods) using the same τ_{qp} and τ_{p} (and same Thouless energy) for both frequencies. Only the bath temperature was allowed to vary. The Thouless energy is expressed as $E_T = \text{hvF/L} \simeq 1.5 k_B K$, taking $v_F \simeq 4.10^5 \, \text{m s}^{-1}$ and junction length $L \simeq 2 \,\mu\text{m}$. **e**,**g**, Corresponding theoretical switching currents computed with $k_B T_b / E_T = k_B T_{qp} / E_T = 0.4$, $\omega \tau_1 = \omega \tau_2 = 0.42$ and $\omega \tau_p = 0.073$.

f,h, Corresponding theoretical occupation probabilities computed with $k_{\rm B}T_{\rm b}/E_{\rm T}=k_{\rm B}T_{\rm qp}/E_{\rm T}=0.7$, $\omega\tau_{\rm 1}=\omega\tau_{\rm 2}=4.6$, $\omega\tau_{\rm p}=0.8$. The corresponding times are $\tau_{\rm ep} = 10.7$ ms and $\tau_{\rm p} = 1.9$ ms. The theory reproduces the intermediate switching branch and its extension with increasing ramp frequency, corresponding to a shift in phase of p_{eg} , relatively well. All occupation probabilities are also well reproduced. The asymmetry of the switching current distribution, reflecting the finite relaxation times, is visible in a and c because of the presence of the intermediate distribution. Correspondingly, the asymmetric shapes of the occupation probability peaks (or dips) are clearly visible in experiment (b,d) and theory (f,h). The model fails, however, to capture some experimental features at 187 Hz. In the experiment in c. the main branch is asymmetric towards positive current, whereas the intermediate, fainter branch is asymmetric towards negative current. In the switching statistics generated by theory, by contrast (g), the main branch extends further, for both positive and negative current, than the intermediate branch. This discrepancy may be attributed to our restricting the model to the first excited state only, see Fig. 2b.

 $p_{\rm eg}$ was less than 5%. Additionally, its maximum is shifted with respect to the p_{ee} and p_{gg} extrema. This situation, with very little poisoning, is unexpected because it corresponds to a higher probability of the more energetic ee state than the eg state. It can be reproduced using a slow pair relaxation time and a relaxation time τ_2 out of the ee state and into the eg state that is ten times longer than the relaxation time τ_1 out of eg and into gg (Fig. 3c). In addition, a much smaller quasiparticle temperature is required than the pair bath temperature, along with a small gap in the Andreev spectrum (too small to be detected in the experiment). The parameters are the same, with $\tau_p = 1.82$ ms as previously but $\tau_1 = 25$ ms and $\tau_2 = 250$ ms. Given the larger number of parameters involved, we considered the description of this low poisoning regime to be qualitative, rather than quantitative (see Supplementary Figs. 7 and 8 for the comparison of experimental and theoretical switching current histograms, integrated histograms and probability distributions for both field regions and both sweep rates).

Our analysis has led to the identification of three times that describe the intra-hinge relaxation from the excited to the ground state within a single hinge (single-quasiparticle or poisoning process, with times τ_1 and τ_2) and the inter-hinge or pair relaxation involving a

two-particle process in which two hinges simultaneously acquire or release a quasiparticle over a time τ_p . This process is impeded if the hinges are far apart, and, correspondingly, τ_p should increase with the separation between hinges. Let us compare the values of τ_p and τ_{qp} we found (albeit overestimated because of possible inductance effects; see Supplementary Figs. 9 and 10) in the ~10-100 ms range to the values obtained in non-topological junctions in similar environments. The poisoning relaxation times we found are similar to those measured in Josephson junctions based on atomic contacts 17,30 and semiconducting nanowires^{31,32}, which vary between a few hundred microseconds and milliseconds. In striking contrast, $\tau_{\rm p}$ estimated in previous studies and associated with the T_1 relaxation time of the Andreev qubit³³ is two to three orders of magnitude shorter, in the microsecond range, than what we found in the Bi nanowire. We interpret this as demonstrating a strong decoupling between hinges, confirming the topological character of Bi. Indeed, whereas in a non-topological Josephson junction every helical channel locally coexists with its opposite helicity counterpart, in a topological system, the two helical channels are spatially separated, typically by 100 nm or more. This separation is roughly 100 times greater than the transverse extension of the helical

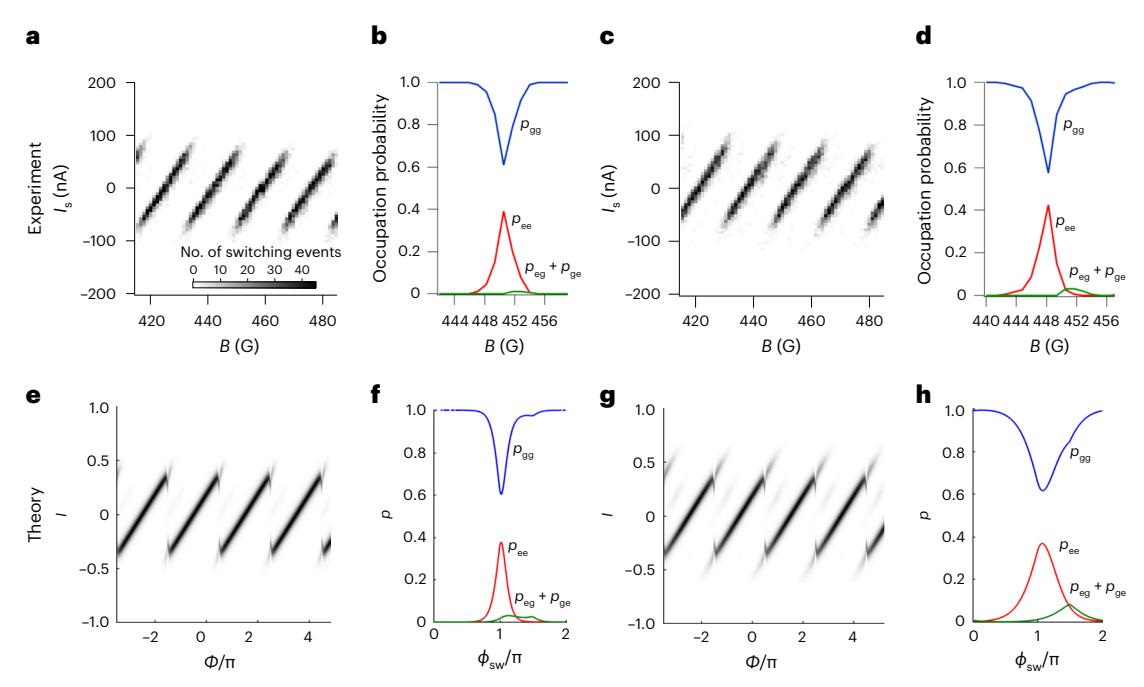


Fig. 5 | Comparison of the experimental switching statistics and extracted Andreev hinge state occupation probabilities to the results of the theoretical model in a field region centred at 450 G. a–d, Experiment. e–h, Theory. a,c, Switching current histograms over four flux periods at ramp frequencies of 17 Hz (a) and 187 Hz (c). A linear dependence has been subtracted to remove the critical current of the strong junction. The intermediate switching current branch is practically not visible. b,d, Field dependence of the occupation probability of the Andreev hinge states extracted from the integrated distributions (see for example Fig. 1f). The occupation probabilities are almost entirely distributed between the ground ($p_{\rm gg}$, blue curve) and excited ($p_{\rm ee}$, red curve) states.The

statistical error on all quantities is $1/\sqrt{N}\simeq 7\%$, where N=200 is the number of measurements at each flux. **e-h**, The corresponding theoretical curves (switching current distribution **e,g**, and occupation probabilities **f,h**) computed with a small gap in the spectrum, and two different relaxation times for quasiparticles, reproduce the qualitative features of this small-poisoning regime, including slightly increased visibility of the poisoned state at higher sweep rates. The parameters are $k_B T_b/E_T=0.4$, $k_B T_{qp}/E_T=0.01$, $\omega \tau_p=0.073$, $\omega \tau_1=1$ and $\omega \tau_2=10$ at 17 Hz, and $k_B T_b/E_T=1$, $k_B T_{qp}/E_T=0.01$, $\omega \tau_p=0.8$, $\omega \tau_1=11$ and $\omega \tau_2=110$ at 187 Hz, yielding $\tau_p=1.82$ ms, $\tau_1=25$ ms and $\tau_2=250$ ms. The gap in the spectrum δ_{gap} at π is $3k_B T_{qp}$.

Andreev states in the Bi nanowire hinges^{20,23}, and 10 times greater than the superconducting coherence length of the disordered W contacts (typically a few nanometres). A remaining puzzle is why the degree of poisoning depends on magnetic field, so that poisoning is clear in one field range and practically undetectable in another. One possibility is that the Zeeman field, by tilting the spins, can remove the orthogonality between the states of a given hinge, thereby allowing spin-conserving and backscattering relaxation/poisoning transitions within one hinge. In contrast, when the states are orthogonal, backscattering relaxation must occur through a change in hinge, which is very slow if the hinges are separated. A second possibility, mentioned in ref. 13, explains the change in effective temperature of the poisoning quasiparticles T_{on} through a change in the nature and number of quasiparticles that can couple to Andreev bound states. Depending on the magnetic field, the Andreev bound states (whose energies shift with the Zeeman field) could be alternately coupled to the quasiparticle continuum above the superconducting gap (yielding a relatively high temperature) or coupled only to rarer localized states (corresponding to a very low temperature). We believe that both the number of available quasiparticles and the selection rules given by the helical nature of the hinges could explain the two very different regimes we saw.

In conclusion, our investigation of the full switching current statistics of a Bi nanoring Josephson junction provides insight into SOTIs and the helical Andreev bound states that are predicted to carry the supercurrent along spatially separated 1D hinges. Our detection around phase π of switching events originating from both excited and ground states, on millisecond timescales, is a demonstration of slow relaxation of quasiparticles and, more spectacularly, of pairs. These features are an unambiguous signature of the topological protection provided by

parity conservation in quantum spin Hall state-based Josephson junctions, opening new possibilities for the design of protected qubits³⁴. In addition, the SOTI hypothesis of transport occurring through two Andreev hinge states of opposite helicities situated at two separate hinges is confirmed by the unusually long pair relaxation time compared with that of non-topological materials. We believe that the full statistical measurement of the switching current is a simple, yet powerful, technique that will prove useful to investigate topology and correlations between current-carrying paths in a vast range of Josephson junctions, particularly those based on 2D TIs and other SOTI materials such as WTe₂ (ref. ³⁵) and Cd₃As₂ (ref. ³⁶).

Online content

Any methods, additional references, Nature Portfolio reporting summaries, source data, extended data, supplementary information, acknowledgements, peer review information; details of author contributions and competing interests; and statements of data and code availability are available at https://doi.org/10.1038/s41567-022-01858-8.

References

- 1. Kane, C. L. & Mele, E. J. Z_2 topological order and the quantum spin Hall effect. *Phys. Rev. Lett.* **95**, 146802 (2005).
- 2. Bernevig, B. A., Hughes, T. L. & Zhang, S.-C. Quantum spin Hall effect and topological phase transition in HgTe quantum wells. *Science* **314**, 1757–1761 (2006).
- 3. Schindler, F. et al. Higher-order topological insulators. *Sci. Adv.* **4**, eaat0346 (2018).
- Song, Z., Fang, Z. & Fang, C. (d-2)-dimensional edge states of rotation symmetry protected topological states. *Phys. Rev. Lett.* 119, 246402 (2017).

- Langbehn, J., Peng, Y., Trifunovic, L., von Oppen, F. & Brouwer, P. W. Reflection-symmetric second-order topological insulators and superconductors. *Phys. Rev. Lett.* 119, 246401 (2017).
- Kwon, H.-J., Sengupta, K. & Yakovenko, V. M. Fractional ac Josephson effect in p- and d-wave superconductors. *Eur. Phys. J. B* 37, 349–361 (2004).
- Fu, L. & Kane, C. L. Josephson current and noise at a superconductor/quantum-spin-Hall-insulator/superconductor junction. *Phys. Rev. B* 79, 161408 (2009).
- Zhang, F. & Kane, C. L. Time-reversal-invariant Z₄ fractional Josephson effect. *Phys. Rev. Lett.* 113, 036401 (2014).
- Peng, Y., Vinkler-Aviv, Y., Brouwer, P. W., Glazman, L. I. & von Oppen, F. Parity anomaly and spin transmutation in quantum spin Hall Josephson junctions. *Phys. Rev. Lett.* 117, 267001 (2016).
- Bocquillon, E. et al. Gapless Andreev bound states in the quantum spin Hall insulator HgTe. Nat. Nanotechnol. 12, 137–143 (2017).
- Deacon, R. S. et al. Josephson radiation from gapless Andreev bound states in HgTe-based topological junctions. *Phys. Rev. X* 7, 021011 (2017).
- Murani, A. et al. Microwave signature of topological Andreev level crossings in a bismuth-based Josephson junction. *Phys. Rev. Lett.* 122, 076802 (2019).
- Lee, S.-P., Michaeli, K., Alicea, J. & Yacoby, A. Revealing topological superconductivity in extended quantum spin Hall Josephson junctions. *Phys. Rev. Lett.* 113, 197001 (2014).
- Peng, Y., Pientka, F., Berg, E., Oreg, Y. & von Oppen, F. Signatures of topological Josephson junctions. *Phys. Rev. B* 94, 085409 (2016).
- Frombach, D. & Recher, P. Quasiparticle poisoning effects on the dynamics of topological Josephson junctions. *Phys. Rev. B* 101, 115304 (2020).
- Crépin, F. & Trauzettel, B. Parity measurement in topological Josephson junctions. Phys. Rev. Lett. 112, 077002 (2014).
- Zgirski, M. et al. Evidence for long-lived quasiparticles trapped in superconducting point contacts. *Phys. Rev. Lett.* **106**, 257003 (2011).
- Beenakker, C. W. J., Pikulin, D. I., Hyart, T., Schomerus, H. & Dahlhaus, J. P. Fermion-parity anomaly of the critical supercurrent in the quantum spin-Hall effect. *Phys. Rev. Lett.* 110, 017003 (2013).
- Schindler, F. et al. Higher-order topology in bismuth. Nat. Phys. 14, 918–924 (2018).
- Li, C. et al. Magnetic field resistant quantum interferences in Josephson junctions based on bismuth nanowires. *Phys. Rev. B* 90, 245427 (2014).
- Drozdov, I. K. et al. One-dimensional topological edge states of bismuth bilayers. *Nat. Phys.* 10, 664–669 (2014).
- 22. Takayama, A., Sato, T., Souma, S., Oguchi, T. & Takahashi, T. One-dimensional edge states with giant spin splitting in a bismuth thin film. *Phys. Rev. Lett.* **114**, 066402 (2015).

- Murani, A. et al. Ballistic edge states in bismuth nanowires revealed by SQUID interferometry. Nat. Commun. 8, 15941 (2017).
- 24. Jäck, B. et al. Observation of a Majorana zero mode in a topologically protected edge channel. *Science* **364**, 1255–1259 (2019).
- Kumar Nayak, A. et al. Resolving the topological classification of bismuth with topological defects. Sci. Adv. 5, eaax6996 (2019).
- Aggarwal, L., Zhu, P., Hughes, T. L. & Madhavan, V. Evidence for higher order topology in Bi and Bi_{0.92}Sb_{0.08}. Nat. Commun. 12, 4420 (2021)
- Cayssol, J., Kontos, T. & Montambaux, G. Isolated hybrid normal/ superconducting ring in a magnetic flux: from persistent current to Josephson current. *Phys. Rev. B* 67, 184508 (2003).
- Delagrange, R. et al. Manipulating the magnetic state of a carbon nanotube Josephson junction using the superconducting phase. *Phys. Rev. B* 91, 241401 (2015).
- 29. Crépin, F. & Trauzettel, B. Flux sensitivity of quantum spin Hall rings. *Phys. E* **82**, 185–190 (2016).
- 30. Olivares, D. G. et al. Dynamics of quasiparticle trapping in Andreev levels. *Phys. Rev. B* **89**, 104504 (2014).
- Hays, M. et al. Direct microwave measurement of Andreev-bound-state dynamics in a semiconductor-nanowire Josephson junction. *Phys. Rev. Lett.* 121, 047001 (2018).
- 32. Hays, M. et al. Coherent manipulation of an Andreev spin qubit. *Science* **373**, 430–433 (2021).
- Janvier, C. et al. Coherent manipulation of Andreev states in superconducting atomic contacts. Science 349, 1199–1202 (2015).
- 34. Hsu, Chen-Hsuan, Stano, P., Klinovaja, J. & Loss, D. Majorana Kramers pairs in higher-order topological insulators. *Phys. Rev. Lett.* **121**, 196801 (2018).
- 35. Kononov, A. et al. One-dimensional edge transport in few-layer WTe₂. Nano Lett. **20**, 4228–4233 (2020).
- Li, Cai-Zhen et al. Reducing electronic transport dimension to topological hinge states by increasing geometry size of Dirac semimetal Josephson junctions. *Phys. Rev. Lett.* 124, 156601 (2020).

Publisher's note Springer Nature remains neutral with regard to jurisdictional claims in published maps and institutional affiliations.

Springer Nature or its licensor (e.g. a society or other partner) holds exclusive rights to this article under a publishing agreement with the author(s) or other rightsholder(s); author self-archiving of the accepted manuscript version of this article is solely governed by the terms of such publishing agreement and applicable law.

© The Author(s), under exclusive licence to Springer Nature Limited 2023

Methods

Bi nanoring-based SQUID

Few-defect monocrystalline Bi nanowires were grown by sputtering high-purity Bi onto a Si substrate covered by a thin layer of vanadium ($T \simeq 70$ °C). The shock wave of short laser pulses was used to shake off nanowires, as in ref. 37, and transfer them contactlessly onto a substrate with prepatterned markers. A few nanowires coiled into rings during the transfer. We selected the loop-shaped Bi nanowire shown in Fig. 1a and followed its crystalline orientation at several points along the ring using electron backscatter diffraction. As represented by the light blue arrows in Fig. 1a, the [111] crystal axis rotated along the ring in an almost radial orientation. An idealized section of the ring is sketched in Fig. 3a, with the helical hinge channels characteristic of SOTIs. The ring was contacted using gallium focused-ion-beam-assisted deposition of a superconducting tungsten compound, after Ga etching to remove the oxide layer covering the Bi surface. The tungsten compound is a disordered superconductor, with a gap $\Delta \approx 1$ meV and a critical field higher than 8 T. On the basis of a careful analysis of several samples using energy-dispersive spectroscopy and etching, we can assert that tungsten contamination extended less than $d \simeq 300$ nm around the deposition regions. The tungsten contacts were connected to thick titanium-gold electrodes.

Switching current measurements

Measurements were carried out in a dilution refrigerator with a base temperature of 100 mK via low-pass-filtered lines and RC filters with a cutoff frequency of ~10 kHz. A magnetic field of up to 12 T was applied perpendicular to the sample plane. The switching current was measured using a counter synchronized with a current ramp of frequency 17 or 187 Hz, triggered by a voltage jump each time the system switched from the supercurrent-carrying state to the resistive state (see the Supplementary Information for more details). A total of 250 (200) switching events were recorded for each value of magnetic field to measure the average (full distribution of the) switching current.

From experimental supercurrent switching statistics to occupation probabilities

The occupation probabilities were extracted from the integrated switching current distributions (Fig. 1f,i) by observing that each step in the integrated distribution corresponded to a transition out of a specific supercurrent-carrying state. The height of the step from one plateau to the next, therefore, counted the number of switching events from that state and was normalized to yield the occupation probability of that state just before the switching event.

Sequence of resolution of the phenomenological model

The theoretical model first generated the occupation probabilities $p_{\rm gg}$, $p_{\rm eg}$ and $p_{\rm ee}$ as a function of $\phi_{\rm sw} = \Phi + \gamma_{\rm max}$ where $\gamma_{\rm max} = \pi/2$. These are displayed in Figs. 4f,h and 5f,h. The switching current probability P(I) and its derivative dP/dI were then generated (as shown in Supplementary Figs. 7 and 8) from which a switching current histogram was created (Figs. 4e,g and 5e,g).

Data availability

The switching current data are available via Zenodo at https://doi. org/10.5281/zenodo.7119795.

Code availability

The MATLAB files for calculating the joint probabilities and switching histograms are available via GitHub at https://github.com/pengyangraul/BiJunction_Codes.

Reference

37. Yu, A. et al. Supercurrents through single-walled carbon nanotubes. *Science* **284**, 1508–1511 (1999).

Acknowledgements

We acknowledge useful discussions with M. Aprili, C. Girit, M. Houzet, J. Meyer, H. Pothier, P. Simon and C. Urbina, technical help from S. Autier-Laurent and funding from the French programme ANR JETS (ANR-16-CE30-0029-01), the European Research Council (ERC) under the European Union's Horizon 2020 research and innovation programme (grant Ballistop agreement no. 833350), LabEx PALM (ANR-10-LABX-0039-PALM) JosephBismuth, CRC 183 (project CO2) of Deutsche Forschungsgemeinschaft (Y.O. and F.v.O.), the European Union's Horizon 2020 research and innovation programme (grant agreement LEGOTOP no. 788715) (Y.O.), ISF Quantum Science and Technology (grant no. 2074/19) (Y.O.) and a BSF and NSF grant (2018643) (Y.O.). Y.P. is supported by an NSF grant (no. PHY-2216774) and the startup fund from California State University, Northridge.

Author contributions

A.K. and V.T.V. grew the Bi nanowires and A.K. deposited them on the substrate. Yu.A.K. characterized the nanowire growth. F.F., A.B. and A.K. selected the nanowires and connected them using focused-ion-beam-assisted deposition. A.B. conducted the low-temperature measurements with input from M.F., R.D., S.G. and H.B. A.B., M.F., R.D., S.G., H.B., Y.P., F.v.O. and Y.O. analysed the data and discussed the results. Y.P., F.v.O. and Y.O. developed the model, and Y.P. wrote the code. S.G., H.B., A.B., R.D., Y.P., F.v.O. and Y.O. wrote the paper.

Competing interests

The authors declare no competing interests.

Additional information

Supplementary information The online version contains supplementary material available at https://doi.org/10.1038/s41567-022-01858-8.

Correspondence and requests for materials should be addressed to S. Guéron.

Peer review information *Nature Physics* thanks Mercedeh Khajavikhan and the other anonymous reviewer(s) for their contribution to the peer review of this work.

Reprints and permissions information is available at www.nature.com/reprints.